Gravimetric and density profiling using the combination of surface acoustic waves and neutron reflectivity

Toolan, Daniel T W; Barker, Robert; Gough, Tim; Topham, Paul D.; Hows e, Jonathan R.; Glidle, Andrew

Published in:
Journal of Colloid and Interface Science

DOI:
10.1016/j.jcis.2016.10.039

Publication date:
2017

Journal of Colloid and Interface Science 487 (2017) 465–474

Contents lists available at ScienceDirect

Journal of Colloid and Interface Science

journal homepage: www.elsevier.com/locate/jcis

Gravimetric and density profiling using the combination of surface acoustic waves and neutron reflectivity

Daniel T.W. Toolan [a], Robert Barker [b,1], Tim Gough [c], Paul D. Topham [d], Jonathan R. Howse [a,*], Andrew Glidle [e,*]

[a] Department of Chemical and Biological Engineering, University of Sheffield, Sheffield S1 3JD, UK
[b] Institut Laue-Langevin, 71 Avenue des Martyrs, 38042 Grenoble Cedex 9, France
[c] School of Engineering, University of Bradford, Bradford BD7 1DP, UK
[d] Aston Institute of Materials Research, Aston University, Birmingham B4 7ET, UK
[e] Division of Biomedical Engineering, Rankine Building, University of Glasgow, Glasgow G12 8QQ, UK

GRAPHICAL ABSTRACT

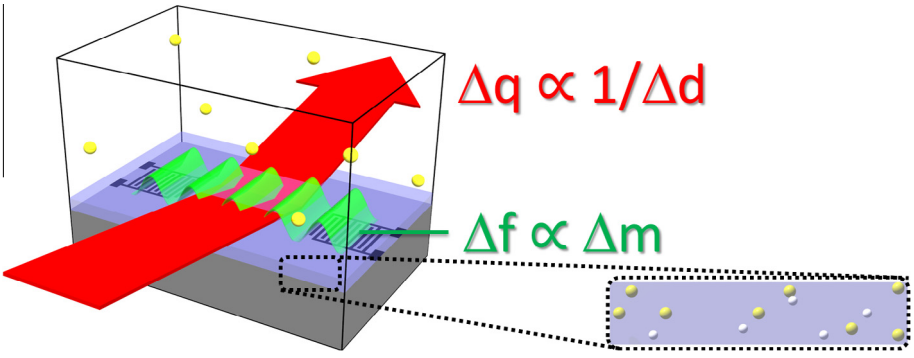

ARTICLE INFO

Article history:
Received 15 August 2016
Revised 14 October 2016
Accepted 18 October 2016
Available online 22 October 2016

Keywords:
Neutron reflectivity
Love wave gravimetry
Interfacial characterisation
Thin film microstructure

ABSTRACT

A new approach is described herein, where neutron reflectivity measurements that probe changes in the density profile of thin films as they absorb material from the gas phase have been combined with a Love wave based gravimetric assay that measures the mass of absorbed material. This combination of techniques not only determines the spatial distribution of absorbed molecules, but also reveals the amount of void space within the thin film (a quantity that can be difficult to assess using neutron reflectivity measurements alone). The uptake of organic solvent vapours into spun cast films of polystyrene has been used as a model system with a view to this method having the potential for extension to the study of other systems. These could include, for example, humidity sensors, hydrogel swelling, biomolecule adsorption or transformations of electroactive and chemically reactive thin films. This is the first ever demonstration of combined neutron reflectivity and Love wave-based gravimetry and the experimental caveats, limitations and scope of the method are explored and discussed in detail.

Abbreviations: NR, Neutron Reflectivity; QCM, Quartz Crystal Microbalance; ATR-FTIR, Attenuated Total Reflection Fourier Transform Infra-Red; RAIRS, Reflectance Absorbance Infra-Red Spectroscopy; XPS, X-ray Photoelectron Spectroscopy; Nb, neutron scattering length density; SAW, Surface Acoustic Wave; IDTs, Interdigitated Transducer electrodes; PMMA, poly methyl methacrylate; VNA, Vector Network Analyser; PECVD, plasma-enhanced chemical vapour deposition; d-PS, deuterated polystyrene.

* Corresponding authors.
E-mail address: andrew.glidle@gla.ac.uk (A. Glidle).
[1] Current address: School of Science and Engineering, University of Dundee, Dundee DD1 4HN, UK.

http://dx.doi.org/10.1016/j.jcis.2016.10.039
0021-9797/

1. Introduction and background

Of the tools available to the soft matter scientist, those which offer information about the material at a buried interface are often the most challenging, yet also the most insightful and meaningful; for example, the study of biomolecules adsorbing at the solid/liquid interface [1], intermixing of polymer layers [2] or chemical transformations of thin films [3,4]. Neutron Reflectivity (NR) is one of the few techniques that can probe the regions below, and at, interfaces in a non-destructive manner. Since model fitting to NR data is used to deduce the structure of the interfacial region, these measurements are often complemented by *ex situ* experiments to provide constraints on the possible model fits. Typically, in such experiments, a similar interface is recreated (or at least approximated) and investigated under similar conditions and parameters. Examples of such complementary techniques include Quartz Crystal Microbalance (QCM) gravimetry, Ellipsometry, Attenuated Total Reflection Fourier Transform Infra-Red (ATR-FTIR) or Reflectance (RAIRS) Spectroscopy and X-ray Photoelectron Spectroscopy (XPS) [3–6]. Each of these techniques allows for the gathering of different types of information which can be used to inform the fitting of NR data, resulting in a deeper, more comprehensive understanding of the interface and layer structure.

5In general, NR reveals, through fitting of data, information about the neutron refractive index profile normal to the reflecting interface. This, in turn, provides insights into the film thickness, density and material composition profiles; importantly, calculation of the neutron refractive index (or the related quantity, neutron scattering length density, Nb) is solely determined by the concentration of the different atoms in the material, and not on any interactions between them. There are analogies with ellipsometry experiments, which provide instead electromagnetic (optical) refractive index and thickness information. However, in contrast to the neutron scattering length density of a material, the value of its optical refractive index is dependent on (bonding) interactions between atoms in the material, which can make the relating of ellipsometric data to the material composition a complex or problematic task [7].

Recently, works have reported experimental approaches that have enabled NR experiments to be performed in parallel or simultaneously, with either ellipsometry [8] or ATR-FTIR [4] measurements. Crucially, the availability of this concurrently acquired data has provided insights into the underlying causes of the changes observed in the NR and corresponding Nb profiles. In addition, usefully, information from these parallel measurements can also be used to distinguish between two similarly good model Nb fits to the NR data; this can be particularly important when performing kinetic NR experiments in which confidence in different model fits is limited by the NR statistics and lack of contrast variations. An illustration of the importance of being able to combine suitable techniques can be seen in the relatively recent provision of a dedicated combined ATR-FTIR-NR beamline for the study of biological and soft matter systems [9].

For many experiments in which the identity of the species adsorbing at the solid/liquid interface is known (e.g. lipid adsorption), there is less need for information about the particular chemical species present. However, what is required is any information that can be used to directly indicate the amount of material that is present at the interface; this can be used to directly inform and complement the fitting of the NR data. As with the combination of NR with ATR or ellipsometry, the requirements of any such *in situ* technique are; (i) it should be easily implemented within the conventional experimental setup on NR beamlines; (ii) allow for standard surface modification chemistries, such as silanes and thiols; (iii) provide quantitative data and (iv) offer temporal resolution at, or greater than, that of the NR beamline.

Currently, the *in situ* combination of QCM gravimetry (which would yield data concerning the amount of a known species) with NR measurements is not feasible because, typically, QCM substrates are of the order of a few hundred microns thick with lateral dimensions of 1–2 cm and sensing areas of ~5 mm diameter. Whilst in theory this is thick enough for an NR substrate, especially with recent developments in data handling [8], the time required for NR acquisition from such small substrates would be considerably longer (>3 h) than is considered interesting for soft matter systems. However, as described herein, an alternative gravimetric technique based on a Love wave Surface Acoustic Wave (SAW) device is ideally suited to combination with NR measurements.

Love wave gravimetry is a well-established analytical technique that has a surface mass sensitivity on the ng/cm^2 scale and can be carried out in either a liquid or dry environment [10,11]. As with the QCM technique, Love wave gravimetry requires a piezoelectric substrate and the most commonly used materials are lithium niobate, lithium tantalate and ST-cut quartz. Importantly, in contrast to the bulk acoustic wave QCM technique, the use of *surface* acoustic waves means that the substrates can be arbitrarily thick (mm), yet with much thinner surface layers (*vide infra*). Thus, in the experiments herein, we have opted to use 1 cm thick ST-cut quartz substrates to take advantage of the availability of high quality, well-polished, flat single crystal quartz substrates (N.B. the neutron absorbance of lithium niobate is ≫50%/cm for wavelengths >2 Å, making it impractical as an NR substrate).

Love wave sensors employ acoustic waves propagating along a thin (1–6 μm) layer of material that is deposited on top of the piezo-active substrate (Fig. 1). The acoustic waves are launched into this waveguide by generation of a *surface* acoustic wave in the piezoelectric substrate using a set of Interdigitated Transducer electrodes (IDTs). Various types of material have been used to construct these waveguides, including SiO_2 and poly(methyl methacrylate) (PMMA) [11,12]. The prime requirements for this layer include low acoustic losses and a lower acoustic velocity compared to that of the underlying quartz substrate. In addition, when used in a sensing context, particularly in liquids, the waveguide material should be robust and not dissolve in, or absorb any of the solvents used in the experimental system.

In a Love wave device, the characteristic resonance frequency of the system is determined by the acoustic velocities in the substrate and a thin waveguide layer, together with the acoustic coupling between them. The spacing between the fingers of the IDT electrodes is then designed so that the acoustic wave generated is in the vicinity of the resonance frequency (see Experimental Section). To measure the amount of material deposited on the surface of the guiding layer, a receiving IDT is used to detect an acoustic wave launched from a transmitting one (Figs. 1 and S1, ESI). In general, small changes in adsorbed mass lead to changes in the acoustic velocity of the waveguide layer and thus a change in resonance frequency of the system.

In practice, Love wave sensor measurements are carried out either by using custom-designed electronic circuits, or by connecting the transmitting and receiving IDT electrodes to the source and detection channels of a Vector Network Analyser (VNA). When using a VNA, the frequency is swept over a range that includes the Love wave resonance frequency. The resolution of the VNA is such that changes in this resonance frequency can be detected with an accuracy of 10–100 Hz.

As with a QCM, with Love wave sensors, there is a direct correlation between the mass adsorbed at the surface and the shift in frequency, Δf, providing viscoelastic losses are negligible (if not, a more complex analysis is required to extract mass data [13]). Furthermore, since $\Delta f \propto f^2$ where f is the base frequency of the

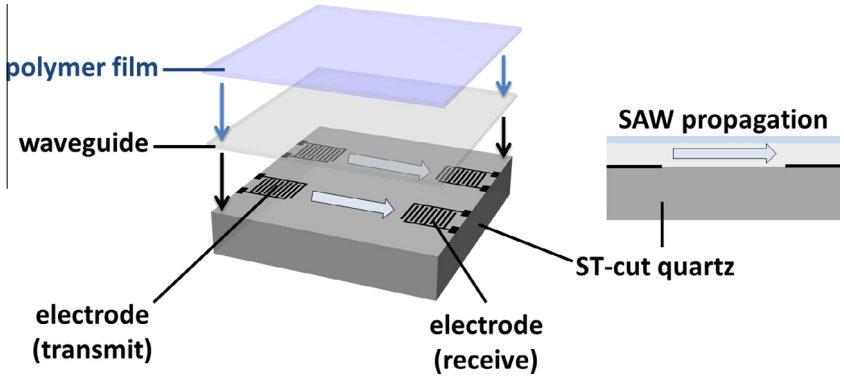

Fig. 1. A schematic showing the components of a Love wave device, showing two electrode pairs, the ST-cut quartz substrate, the amorphous capping quartz waveguide and the additional polymer film as used in this study.

oscillator (as in the Sauerbrey equation), and since Love wave devices usually operate at a higher frequency than QCMs, they have an inherently greater mass sensitivity. For acoustic resonators, the mass sensitivity, S, is often defined as shown in Eq. (1) [14].

$$S = \left(\frac{\Delta f}{f}\right) \Big/ \left(\frac{\Delta m}{A}\right) \quad (1)$$

where Δf is the frequency change observed when a mass change, Δm, occurs over an area, A.

Here, we report for the first time, measurements that combine the NR and Love wave techniques in order to correlate mass changes (Δm) in an adsorbed layer, with the solvation and microstructural profile of that layer. To establish and illustrate this method, the question that we sought to answer was whether the combination of the two techniques could be used to provide complementary data that could be used to determine the void (air filled) space within a spun polymer film, before and after it is exposed to solvent vapours that lead to polymer swelling. This will give insights into the factors determining the maximum level of vapour uptake in systems such as those often employed as gas, vapour or humidity sensors.

Traditionally, NR investigations of void or air space have been conducted using hydrogenous and deuterated versions of the solvent and polymer, where available. However, for many organic polymers, the Nb contrasts between the hydrogenous polymer, hydrogenous solvent and air are small, leading to uncertainties in the model fitting, especially if the polymer interfaces are diffuse. As shown below, the ready means of correlating Δm_{LW} as determined by the Love wave device, with film parameters determined by model fitting to the NR data, demonstrate the suitability of combining the Love wave technique with NR experiments to give a more complete description of the film structure, without the need for expensive or not readily available deuterated components.

The system we have opted to use to establish this novel methodology uses thin films of polystyrene exposed to solvent vapours of either acetone or chloroform. The absorption of vapours into this model system has been well studied by both neutron and X-ray reflectivity. For example, in both the X-ray [15] and NR [16] studies of CO_2 uptake, the authors drew conclusions about the distribution of CO_2 within PS films when exposed to various pressures of CO_2. However, for both these cases, knowledge of the amount of CO_2 absorbed into the films (using a method such as that outlined below) could have helped the authors evaluate the accuracy of the model density profiles presented (n.b. neither study appeared to consider the possibility of there being void space in the film).

2. Materials and methods

2.1. Love wave device preparation

As shown in Figs. 1 and S1, the Love wave structure comprises an ST cut block of quartz onto which four pairs of gold IDT electrodes are first fabricated, followed by PECVD deposition of an amorphous, isotropic 2 μm thick SiO_2 layer. The ST quartz block (100 mm × 50 mm × 8 mm) was initially polished to λ/10 (Gooch and Housego, UK) and cleaned by ultrasonication in acetone followed by propan-2-ol, prior to deposition of the IDT electrode pairs using standard photolithography methods. The centre-centre spacing between adjacent fingers in the IDT array was 20 μm, so as to give a surface acoustic wave frequency of ~120 MHz [12,17]. The IDTs were oriented so that the surface acoustic wave propagated along the z-axis of the ST quartz. Each IDT consisted of 20 pairs of fingers and the centre-centre separation between the transmitting and receiving sets of electrodes was 10 mm (see Supplementary Fig. S1). Although only one pair of transmitting and receiving IDT electrodes is needed to measure the adsorption of material on the surface, we opted to have multiple (4×) electrode pairs, one at each corner of the neutron block. This builds in a level of redundancy and averaging to the Love wave measurements, and could be used to estimate any variations in solvent uptake in different regions of the polymer surface.

Following deposition of the IDT electrodes, a 2 μm thick PECVD film of SiO_2 was deposited on top of these, and the substrate, using an Oxford Instruments 80+ deposition machine. The value of 2 μm was selected as a compromise thickness that allowed reliable fitting of NR data and taking note of the finding that although thicker films SiO_2 films lead to higher mass sensitivity, they can also suffer from delamination problems (see ESI, including Figs. S2 and S3 for discussion on this point).

The Love wave transmit and receive signals were measured using an Agilent 4395a Network Analyser, with an 87512a send/receive attachment. A 1 V p-p AC voltage source was applied to the transmitting IDTs and the frequency swept over a range of either 10 kHz or 120 kHz, centred on the Love wave resonance frequency.

Whilst the sensitivity and scaling relationship between Δf and Δm for a Love wave device can be calculated from theory [12,13], in practice it is best to determine this empirically. Thus, devices were calibrated *ex situ* by spin coating with hydrogenous polystyrene films of varying thickness (and hence masses). The films were annealed at 120 °C for 2 h to remove solvent and consolidate them. The shift in resonance frequency from that of an uncoated Love wave device was then measured and plotted against the thickness of the polymer film determined using a Veeco Dektak

5 M profilometer. In addition to measuring thickness data, transmission UV spectra were collected for the spun PS films on the Love wave devices. This spectroscopic data showed that the absorption bands in the range 220–260 nm scaled linearly with the thickness data, indicating that, for the range of polymer films prepared here, there is no significant change in polymer volume fraction that might influence the mass/frequency calibration data. A typical calibration curve is shown in the ESI, Fig. S4. Note, for accuracy, to analyse the Love wave data associated with the film and block that were used to collect NR data, the Love wave frequency/mass sensitivity factor (S) used was that derived from the calibration data from that specific block (when measuring calibration curves for different Love wave devices on different neutron blocks having similar thicknesses of deposited SiO_2, it was found that they had slopes that correlated well with the actual SiO_2 thickness, as expected).

2.2. In situ vapour absorption experiments

For *in situ* vapour absorption experiments on the neutron beamline, a deuterated polystyrene film (d-PS, Polymer Labs, M_n = 200 - kDa) was deposited on the Love wave substrate by spin casting at 1000 rpm from a 25 mg/ml solution in toluene. Differential interference contrast (DIC) optical microscopy inspection over the whole surface indicated the surface was smooth and with few asperities (on the 100 nm scale). Before the neutron experiments were performed, the film was exposed to acetone vapour and then dried in a stream of dry nitrogen, to check there was a measureable shift in frequency on acetone uptake over a range of vapour pressures. The film was then left (without annealing), for several days to allow any residual toluene to evaporate, prior to exposure to solvent vapours. To generate a controlled solvent rich vapour to swell the polymer film, the gas mixing set-up shown in Fig. 2 was used. A stream of dry nitrogen was first bubbled though the solvent and then mixed with a second dry nitrogen stream before passing into a final vessel to trap any condensing solvent or aerosols. The concentration of the solvent was determined by use of an FTIR gas cell mounted in-line with a neutron reflectivity vapour cell (spectra were recorded every 5 min during the acquisition of the NR profiles to monitor and ensure the solvent vapour concentration remained constant during each measurement run).

The neutron reflectivity vapour cell, housing the Love wave device + d-PS film was a sealed aluminium chamber (ca. 15 cm diameter) fitted with thin aluminium foil windows and electrical feedthroughs connected to the electrode pairs on the block. The quartz block was mounted in a vertical orientation with the longest surface parallel to the beam (see Fig. S1).

2.3. Neutron reflectivity

Neutron reflectivity experiments were carried out on the D17 time-of-flight reflectometer [18] at the Institut Laue-Langevin (ILL), Grenoble, France. Specular reflectivity was measured at two grazing angles of incidence (θ = 0.8° and 3.2°) with an incident neutron beam having a useable wavelength range of 2.0–22.0 Å and the collimation slits before the sample adjusted for each angle to ensure a constant beam footprint on the sample. Data acquisition required 60 min per sample. After correction for the wavelength-dependent transmission through the cell windows, the data for each angle were combined to obtain the complete reflectivity profile. Using two angles of incidence ensured that R (Q) was measured from before the critical edge ($Q_{critical}$ = 0.012 $Å^{-1}$) to the background (Q = 0.2 $Å^{-1}$). After data reduction, fitting was performed using Parrat32 software.

The combined neutron reflectivity and Love wave experiments were conducted in the following stages; (i) gas flow adjusted to establish solvent vapour composition prior to flowing over the sample; (ii) FTIR spectra recorded to monitor solvent concentration in the vapour phase and allow constant solvent concentration during the NR measurements to be maintained, typically this took 10–30 min due to the large vapour volume inside the cell and the low vapour flow rate; (iii) Love wave signal measured; (iv) NR data collection started, and (v) Love wave signal and FTIR spectra measured periodically until the end of NR data collection.

3. Results

Fig. 3 shows the NR data and subsequent fit for the d-PS coated Love wave device, clearly showing uniform fringes resulting from the high scattering length density deuterated polymer. The dry film thickness was determined to be 1403 Å, with an Nb of 6.32×10^{-6} $Å^{-2}$, consistent with spin-coated films of this type but slightly lower than the value of 6.47×10^{-6} $Å^{-2}$, which is based on the bulk density of 1.13–1.14 g/cm^3 for deuterated polystyrene [19,20].

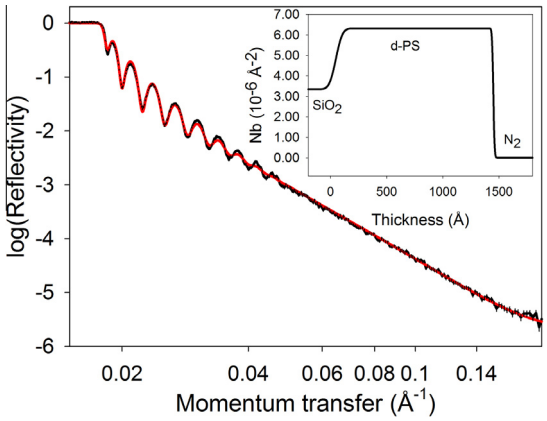

Fig. 3. Neutron reflectivity data of the dry d-PS film on the Love wave device exposed to a stream of pure N_2 (black dots and error bars) together with the corresponding best fit model (red line) and neutron scattering length density (Nb) profile (inset). (Note, raw data error bars are generally obscured by the dot and line thicknesses). (For interpretation of the references to color in this figure legend, the reader is referred to the web version of this article.)

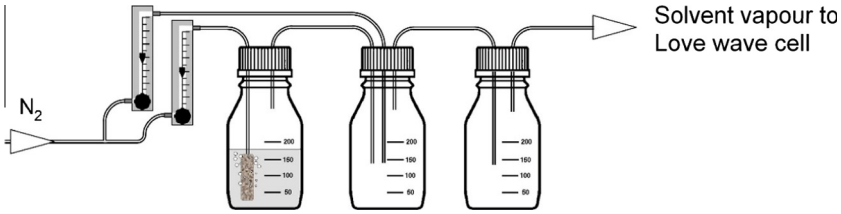

Fig. 2. Schematic showing the set-up used to control the solvent vapour concentration. The centre flask was use to mix the pure N_2 stream with the solvent rich stream, whilst the final flask was used to collect condensing droplets which may have formed.

Fitting indicated that the external (vapour/film) interface was sharp, with roughness of ~9 Å, but that there was a relatively higher roughness (or gradation in material density) at the polymer/SiO_2 interface. This was determined to be ~50 Å and could be attributed it to coating irregularities/thinning, the surface quality of the PECVD deposited oxide, residual stresses at the polymer/substrate interface, or residual solvent from the deposition or previous swelling experiments that was trapped at the polymer/substrate interface (discussed later) [21]. Importantly in the context of the data analysis below, this parameter was held constant when fitting data for the film exposed to different vapour concentrations (the constant value used was determined following a series of fits to each of the reflectivity profiles in which it was allowed to float). Prior to data fitting, the reflectivities were not corrected for an energy dependant absorption of neutrons by the vapour phase since calculations show this effect to be less than 0.05% (in the 2.0–22.0 Å range).

The film was then exposed to a series of acetone or chloroform rich vapours. The range of concentrations used was determined by adjusting the flow through the solvent reservoirs and combining that with a varying amount of a dry N_2 stream. Acetone and chloroform were chosen due to their differing solvating properties, molecular volumes, and densities ($\rho_{Acetone} = 0.786$ g cm^{-3} and $\rho_{CHCl3} = 1.498$ g cm^{-3}). This enabled us to explore the effects of different degrees of solvent-induced swelling and mass loading.

As the solvent vapour concentration is increased, as anticipated, the film swells and consequently the fringes become more closely spaced and move to lower Q (Fig. 4a). Similar changes are seen when the film is exposed to increasing chloroform vapour concentrations (Fig. 4b). In both cases, since the film is absorbing a hydrogenous solvent, the Nb for the film decreases (Fig. 5a and b). Whilst both acetone and chloroform are good solvents for PS, there are clear differences between the two profiles, with the film absorbing and swelling more in the chloroform vapour (for a given vapour concentration). However, due to the order of magnitude difference in the scattering length density between acetone (2.37×10^{-7} Å^{-2}) and chloroform (2.30×10^{-6} Å^{-2}), whilst more chloroform is absorbed into the film, for a given degree of solvent induced swelling, the degree by which the scattering length density of the film reduced is significantly less (see inset Fig. 5b).

To analyse these data sets further, use is made of the equations that relate the overall scattering length density of the swollen film, Nb_{film}, to the Nb of the dry polymer, $Nb_{d\text{-}PS}$, and the Nb of the solvent, Nb_{solv}, through Eqs. (2) and (3):

$$Nb_{film} = \varphi_{d\text{-}PS} \cdot Nb_{d\text{-}PS} + \varphi_{solv} \cdot Nb_{solv} + \varphi_{air} \cdot Nb_{air} \quad (2)$$

$$\varphi_{d\text{-}PS} + \varphi_{solv} + \varphi_{air} = 1 \quad (3)$$

where $\varphi_{d\text{-}PS}$, φ_{solv} and φ_{air} correspond to the volume fractions of the polymer, solvent and air molecules in the film, respectively (N.B. the contribution from the air volume fraction in Eq. (2) is essentially zero, due to the scattering length density of air, Nb_{air}, being close to zero).[2] From equations such as these, in order to determine the volume fractions of the different components using neutron reflectivity alone, measurements would need to be made in at least three different neutron contrasts of the polymer and solvent that give identical degrees of solvent swelling e.g. hydrogenous and deuterated versions of the solvent together with hydrogenous and deuterated versions of the polymer in at least one solvent contrast. (Note, in the case of the experiments performed here, a stream of dry nitrogen, rather than air, was used to carry the vapour into the NR cell, but for simplicity this is referred to simply as 'air' in the equations and text below).

[2] In the case of the experiments performed here, a stream of dry nitrogen, rather than air, was used to carry the vapour into the NR cell, but for simplicity this is referred to simply as 'air' in the equations and text below.

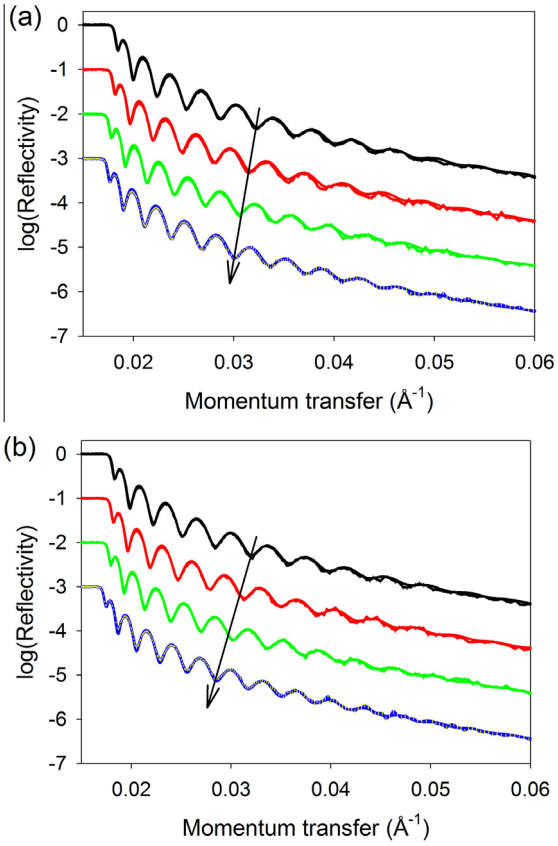

Fig. 4. Selected neutron reflectivity data (coloured dots) and best fit models (coloured lines) showing the fringe movement resulting from the film swelling in (a) acetone and (b) chloroform rich vapour. Acetone concentrations 0 (black), 2300 (red), 72,500 (green) and 143,000 (blue) ppm. Chloroform concentrations 0 (black), 1580 (red), 57,600 (green) and 100,000 (blue) ppm. Arrows indicate the movement Kiessig fringes with increasing vapour induced swelling. (Note, raw data error bars are generally obscured by the dot and line thicknesses). (For interpretation of the references to color in this figure legend, the reader is referred to the web version of this article.)

Carrying out neutron measurements in the different solvent contrasts indicated above is often practical for liquid phase measurements, this is more problematic (or costly) for vapour phase measurements without a specifically constructed vapour generator and cell that consumes low volumes of solvent. (Note, for the NR measurements reported here ~100 ml of liquid solvent were consumed and vented to the atmosphere.) Furthermore, in order to combine variations of Eq. (2) that correspond to different contrasts of the polymer, it would be necessary to be able to prepare H- and D-versions of the polymer film that contained molecules which were closely matched in both length and degree of branching, and could be spun-cast to identical thicknesses. Whilst possible in some instances [22], experimentally, in others, this would be challenging and could lead to unknown degrees of uncertainty when combining measurements from different neutron contrasts.

Instead, if the mass of the solvent absorbed is measured and the scattering length density of the pure (air free) polymer is known (or measured), the average volume fractions of the different components can be extracted by combining these numbers with the integral version of Eq. (2), i.e. Eq. (4), which sums the scattering length contributions of all the components in the film. Eq. (4) can be transformed into Eq. (6) (*via* Eq. (5)) to relate the integrated film scattering length density to the surface coverages (Γ in g/cm^2) of the polymer and solvent.

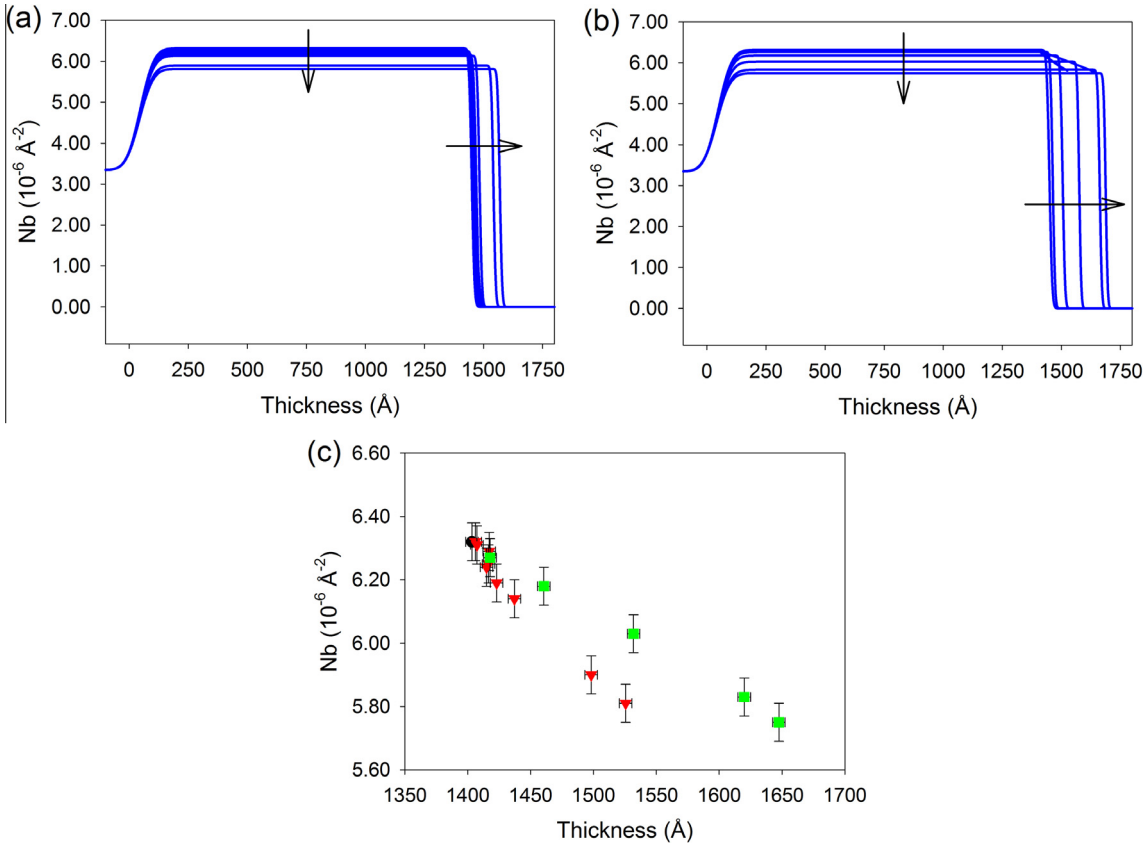

Fig. 5. Neutron scattering length density profiles showing the effect of solvent uptake within the d-PS film for a range of increasing vapour concentrations for (a) acetone and (b) chloroform. The arrows represent the effect of increases in the solvent component within the film. The linear relationship between the change in thickness and change in Nb is a result of the differences in the Nb of the solvents is shown in (c).

$$\int Nb_{film} \cdot dz = \int \varphi_{d\text{-}PS} \cdot Nb_{d\text{-}PS} \cdot dz + \int \varphi_{solv} \cdot Nb_{solv} \cdot dz \tag{4}$$

$$\int Nb_{film} \cdot dz = N_A \cdot \left(\sum b_{i,d\text{-}PS}\right) \cdot \left(\frac{\rho_{d\text{-}PS}}{Mw_{d\text{-}PS}}\right) \cdot d + N_A \cdot \left(\sum b_{i,solv}\right) \cdot \left(\frac{\rho_{solv}}{Mw_{solv}}\right) \cdot d \tag{5}$$

$$\int Nb_{film} \cdot dz = N_A \cdot \left(\sum b_{i,d\text{-}PS}\right) \cdot \left(\frac{\Gamma_{d\text{-}PS}}{Mw_{d\text{-}PS}}\right) + N_A \cdot \left(\sum b_{i,solv}\right) \cdot \left(\frac{\Gamma_{solv}}{Mw_{solv}}\right) \tag{6}$$

where z is the direction perpendicular to the reflecting interface, the b_i's and Mw's are the scattering lengths of the atoms and molecular weights respectively in/of the solvent and d-PS; d is the film thickness and N_A is Avagadro's constant.

The determination of added mass (Γ_{solv} or Δm_{LW}) *via* the Love wave device is relatively straightforward due to the linear relationship between Δm_{LW} and frequency shift (Δf) and the availability of a calibration curve for the device. Similarly, $\Gamma_{d\text{-}PS}$ can be determined either from Love wave data (after removal of the spun film), or from integrating the model fit scattering length density of the film in the dry (solvent free) state.

In the set of Eqs. (2)–(6), the principal quantity that is neither directly measured, nor directly inferred from model fits, is the volume fraction of air, ϕ_{air} within the polymer film. In non-annealed films, such as the one studied here, this air or void space between the folded polymer chains can arise during the slow solvent evaporation in the final phases of spinning and subsequent room temperature drying [23], or from microscopic pinholes that are observed in spun films of these thicknesses.

There are two approaches to extract ϕ_{air}, or the related quantity, d_{air}, the effective thickness of the air component within the film. One approach is to use the NR model-derived film thickness, d_{film}, as in Eq. (7) (*cf.* Eq. (3)) where the bulk density of the polymer and solvent allows you to calculate the notional thickness of these components:

$$d_{air} = d_{film} - d_{d\text{-}PS} - d_{solv} \tag{7}$$

with d_{film}, $d_{d\text{-}PS}$ and d_{solv} being calculated from the neutron and Love wave-determined surface coverages and (void free) densities. The second approach is to use the average model fit for the film Nb, $\langle Nb_{film}\rangle$, together with Eq. (5):

$$d_{air} = (Nb_{d\text{-}PS}d_{pol} + Nb_{solv} \cdot d_{solv} - Nb_{film} \cdot (d_{solv} + d_{pol}))/\langle Nb_{film}\rangle \tag{8}$$

It is noted that if the model fits to the NR data were 'perfect', then the integral equation (Eq. (6)) could be used to calculate the mass uptake when exposed to each of the different vapour concentrations from the neutron data alone. However, when this is done in practice, the integrated scattering length density sometimes increases, and sometimes decreases. This is because of the relatively low contribution to the overall Nb from the absorbed solvent (see later) and small errors in model parameters inherent when using simple model fit profiles. Thus, in order to extract further information from the NR profiles, Nb models were combined with Love wave data sets. In doing this, some assumptions need to be made about the errors associated with the quantities derived from the NR and Love wave data sets. In the case of the best fit Nb model profile, these are associated with the alignment, thickness,

scattering length density of the film, and the interfacial roughnesses. For the Love wave data, these are the position of the resonance frequency (Hz) and the frequency/mass conversion factor. The errors associated with this new approach are discussed in detail throughout the ESI.

When considering the influence of the Nb model profile parameters on NR data such as those in Figs. 3 and 4, the film thickness predominantly determines the fringe spacing. The differences in scattering length density between the film and each of the substrate and air interfaces determines the depth and shape of the fringes, and the interfacial roughnesses determine the shape of the fringes, the degree to which they can be observed at higher Q values and how fast the reflectivity curve decays with increasing Q.

In the case of NR profiles collected on a well-aligned and calibrated time-of-flight machine, such as D17, having a model that fits well to the minima and maxima of each of the 10 fringes in Figs. 3 and 4, indicates that the thickness parameter is very well-defined.

For the Love wave data, measurement of the frequency is accurate to ~100 Hz in the 100 MHz frequency range. This corresponds to an error of ~1% when calculating the frequency shifts in the above vapour adsorption experiments. The other source of error associated with Love wave measurements comes from the frequency/mass conversion factor. Here, two of the factors that need to be considered are the temperature sensitivity and losses associated with the film's viscoelasticity. To examine each of these effects, a series of measurements were carried out to measure the frequency shifts of both dry films of different thicknesses (to evaluate viscoelastic losses) and of a dry film at different temperatures (to determine the temperature dependence of the sensitivity factor, S). This is discussed in detail in the ESI; in short, the resonance frequency shift varied linearly with increased film thickness for films up to ~50 nm and, as the Love wave-based gravimetry is such a sensitive technique, the small changes being measured here require the substrate temperature to be closely controlled. Unfortunately, during our first demonstration of this approach on D17, the ambient temperature varied during the course of the day and thus, whilst the Love wave resonance frequency data was readily collected, the frequency shifts were slightly different to those collected in the laboratory. This problem can be addressed with a more sophisticated sample holder design in future experiments. Consequently, for accuracy in the analysis below, additional Love wave measurements were made, *ex situ*, in a thermally controlled environment (as discussed in detail in the ESI) and are shown in Fig. 6 (note, the concurrent collection of FTIR vapour spectrum during the NR measurements enabled the vapour concentration for the *ex situ* measurements to be set appropriately).

Fig. 6 shows the shifting of the resonance peak with increasing acetone concentration in the surrounding vapour for the d-PS film used in the NR experiments. Similar shifts are seen for chloroform absorption and these can also be converted to an increase in mass per unit area (Fig. 7) using the Love wave device sensitivity constant, S.

A final source of uncertainty in interpreting the measured Love wave data and extracted model Nb profiles comes from consideration of whether or not any solvent is present when the films are in the 'dry' state at the start of the Love wave/NR experiments. In this respect, some of the previously reported NR measurements have indicated that there may be up to 15% v/v toluene present in freshly deposited films [21], whereas the NR (and FTIR) measurements in other reports indicated there was no toluene present [22]. The most likely cause of the discrepancy between these two sets of measurements is the precise way in which the spin-coated polymer films were prepared and stored: differences in spin-coating speed is likely to be a key factor here, since the point at which vitrification occurs will determine whether or not

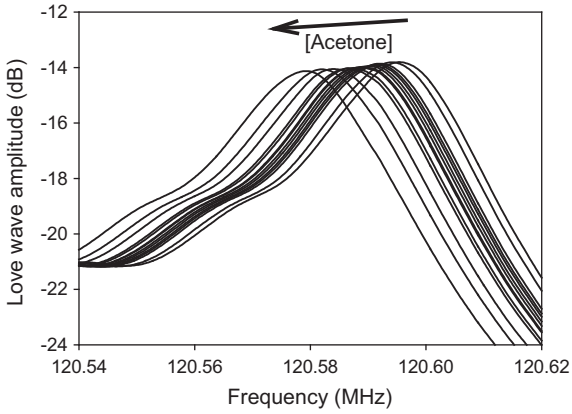

Fig. 6. Love wave frequency response curves, at 25.6 °C ± 0.1 °C, for the d-PS film of Fig. 3 showing the resonance peak and its movement to lower frequencies with solvent uptake (arrow) for vapour phase concentrations of acetone varying from 0 to 200,000 ppm. Similar shifts in the resonance peak are seen with $CHCl_3$ adsorption (see Fig. S5).

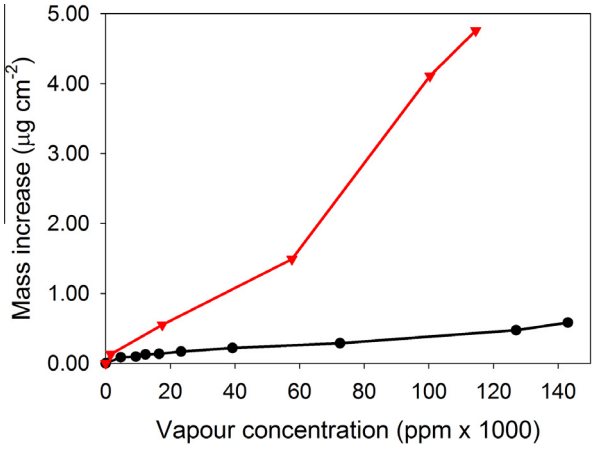

Fig. 7. Mass uptake by the 1400 Å thick spun d-PS film when exposed to acetone (black dots and line) and chloroform (red dots and line) vapours. (For interpretation of the references to color in this figure legend, the reader is referred to the web version of this article.)

residual solvent is present. For the films used here, it was notable that the Love wave frequency for the 'dry' state was constant during the passage of dry nitrogen over the film surface for several hours (>6), thus, the ng/cm^2 sensitivity of the Love wave measurements led to the supposition that a negligible amount of solvent (or water) remained within the film. A possible reason for the solvent content being lower here than that reported elsewhere [21] could be (1) the films studied here spin-coated at a slower speed (leading to a later onset of vitrification) and (2) prior to NR measurements, the films were swollen through exposure to acetone vapour. The effect of a history of swelling in acetone vapour could have been to allow any residual toluene to diffuse out of the film and, since acetone is a 'poor' solvent for polystyrene, any remaining acetone would have been readily removed by the dry nitrogen stream, if it hadn't been lost whilst being stored.

Bearing in mind the aforementioned caveats concerning the accuracy of the NR model derived parameters (discussed in detail in the ESI), to analyse the combined NR-Love wave data sets, both the thickness and model film Nb parameters have been individually combined with the mass data from the Love wave measurements. This allows the effective thicknesses of the polymer, solvent and air fractions in the spun d-PS film of Fig. 3 to be

calculated using Eqs. (7) and (8). The results of these calculations are tabulated in Tables S1–S4 for different acetone and chloroform vapour concentrations. (Note, the scattering length densities of hydrogenous acetone and toluene are sufficiently small compared to deuterated polystyrene, that had the non-polymer volume been occupied by either of these solvents, rather than air, the error in the calculated thickness of the polymer component would be ~0.2%.)

Table 1 (a more detailed table is available as Table S1 in ESI) shows the air component calculated from the model film thickness using Eq. (7) for different degrees of acetone exposure (see Table S3 for corresponding chloroform data); Tables S2 and S4 calculate this component using the average model film Nb (i.e. Eq. (8)). In each of the tables, the model parameter that was not used in the air component calculation is also derived (by back substitution into Eqs. (7) or (8)) and compared with the value of the parameter that had been found from the NR model fit. In nearly all cases, this percentage error is less than 1%. This, together with the closeness in the values of the air components calculated using these two methods (±10 Å), gives a high degree of confidence that these values are consistent with the overall model Nb profile fits.

Whilst the above data suggest that the air component of the film could be upwards of 25 Å thick (depending on the degree of swelling), these estimates are influenced by the alignment accuracy of the NR setup as well as the model fitting. For example, calculations indicate that an alignment error of 1% in the sample angle could lead to an over estimate in the air layer thickness of ~30 Å. Although this would 'remove' the air component from the as-deposited 'dry' film, the data would still suggest an air component was present in the more highly swollen films (even if the 'air' component in the as-deposited 'dry' film, was in fact residual solvent from the spin-coating deposition process). Thus, clearly, when performing measurements such as these, it is important to pay close attention to the sample alignment. In these measurements the sample was not realigned between exposure to different vapour concentrations. This avoided introducing different alignment errors for measurements at different vapour concentrations.

From the data in Table 1 (and Tables S1–S4, ESI), it can be seen that air and vapour volume fractions in the films are relatively small (as expected), corresponding to a few percent (<6%) of the overall film volume. It can also be seen that as the acetone vapour concentration increases so does the thickness of both solvent and air components. This is shown as a change in the volume fraction

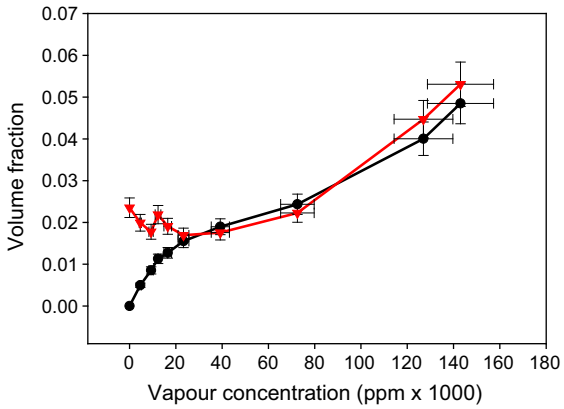

Fig. 8. Changes in volume fraction of acetone (black dots) and air (red dots) components of the d-PS film of Fig. 2 after exposure to acetone vapour in the range 0–143 parts per thousand. (For interpretation of the references to color in this figure legend, the reader is referred to the web version of this article.)

in Fig. 8. The first observation with regard to Fig. 8, is that absorption of small amounts of acetone appears to cause a minimal change in the volume fraction of air. Secondly, it appears that after a certain amount of acetone has been taken up (at 20,000 ppm), the air volume fraction starts to increase at a rate comparable with the increase in solvent volume fraction. If the internal microstructure of the film is pictured at the polymer chain level, and if the cause of the void space in the film is the spacing between individual polymer chain globules, then this could indicate that solvent-induced swelling of the polymer does not cause significant intermixing of these domains. Likewise, if the cause of the air space is the presence of pinhole-like defects, solvent swelling does not cause these to be filled in.

Whilst of less importance for many applications of spun films of PS (used as a model system here), this sort of information about changes in void space in films as they take up vapour, or solvent, is important for systems that are used as sensors e.g. the use of polyimide in commercial humidity sensors. There, the maintenance of space between polymer strands is important in facilitating mass transport through the sensor film, and thus the response and recovery times of the sensor on, or after, exposure to certain levels of water vapour.

Table 1
The thicknesses of polymer and solvent components calculated from model Nb profile fits and Love wave gravimetric data for a d-PS film exposed to increasing concentrations of acetone, together with estimations of the thickness of the air component. The error between the film Nb derived from these thickness estimations and the best fit model Nb parameter is given in the last column.

Acetone vapour concentration	Neutron fitting results			Thickness of polymer component [a]	Love wave: Mass of solvent	Thickness of solvent component [b]	Calculated thickness of air component (voids) [c]	Derived film Nb[d]	Error between derived and model Nb
10^3 ppm	d (Å)	10^6 Nb (Å^{-2})	Roughness (Å)	(Å)	(μg cm^{-2})	(Å)	(Å)	10^6 Nb (Å^{-2})	%
0 (pure N_2)	1403	6.32	9.2	1370	0.000	0	33	6.321	0.0
4.65	1406	6.32	9.7	1370	0.061	7	28	6.311	0.1
9.30	1407	6.31	9.7	1370	0.092	12	25	6.305	0.1
12.3	1417	6.29	10.8	1370	0.124	16	31	6.263	0.4
16.5	1415	6.24	10.1	1370	0.138	18	27	6.273	−0.5
23.3	1417	6.25	8.8	1370	0.173	22	24	6.266	−0.3
39.2	1423	6.19	9.1	1370	0.216	27	25	6.239	−0.8
72.5	1437	6.14	8.2	1370	0.277	35	32	6.179	−0.6
127	1498	5.90	7.7	1370	0.474	60	67	5.932	−0.5
143	1526	5.81	7.7	1370	0.582	74	81	5.827	−0.3

Errors in the film thicknesses, Nb and roughness resulting from fitting and alignment are <10 Å, 0.05 Å^{-2} and 5 Å respectively.
[a] Determined from Eq. (7), assuming a Nb of dPS of 6.47 × 10^{-6} Å^{-2} for a density of 1.13 g cm^{-3}.
[b] Determined from Love wave data, assuming solvent density of 0.791 g cm^{-3}.
[c] Calculated from combination of neutron fitting thickness, polymer content thickness (NR) and solvent thickness (Love wave).
[d] Back-calculated using Eq. (7).

4. Discussion

One of the aims of these experiments was to explore whether Love wave gravimetric data with information gained from model fitting of NR data could be combined to provide new information about the system being studied, and whether a single sample and sample environment could be used for both sets of measurements. The calculations employed herein have indicated that the volume fractions of both air and solvent are small and two methods of calculating these from different parameters associated with the model Nb fits gave very similar results.

The measurements also demonstrated, for the first time, that a single sample and a single sample environment can be used for both the Love wave and NR measurements. However, as can be appreciated from examination of the temperature sensitivity of the Love wave resonance frequency (ESI Fig. S6), performing the Love wave experiments on the neutron beamline requires the ambient and sample holder temperature to be very well controlled.

The second issue concerning the Love wave data can be seen by examining the values of the calculated air component for high values of chloroform absorption (Tables S3 and S4). These appear to suggest that there is a negative amount of air in the polymer film at high chloroform loadings. However, closer scrutiny of the resonance frequency response for the Love device for these degrees of $CHCl_3$ absorption (ESI, Fig. S5) show that there has been a significant loss in transmitted power (compared to that when the polymer absorbs acetone or smaller quantities of chloroform). These viscoelastic losses are also seen in the thickness-resonance frequency calibration plot (ESI, Fig. S4) and indicate that as the film becomes less rigid, the frequency to mass conversion factor becomes smaller. Qualitatively, this would indicate that the mass of absorbed chloroform from high vapour concentrations given in Tables S3 and S4 is an overestimate of the true value. The effect of this overestimate is to decrease the calculated air component (to the extent here that it has become negative).

Thus, in order to use Love wave data in quantitative analysis, care must be taken to ensure that the system studied is sufficiently rigid with low acoustic losses, so that a linear mass-frequency relationship can be used (estimation of mass change when there is an accompanying significant viscoelastic change can be complex).

5. Conclusions

In this work, our hypothesis was that it should be possible to combine information gained from NR and Love wave measurements of a single sample, under identical conditions to yield information that could not be gained from the NR measurements alone. This method, presented here for the first time, has been used to extract details about the internal microstructure of polymer films as they undergo simple transformations (i.e. the presence/appearance of void space in vapour-induced swelling in this demonstration).

When surveying earlier work on the solvent content in thin polymer films in the 'dry' state it can be envisaged that the use of this method would have benefited a number of the neutron and X-ray reflectivity studies. For example, with studies under static (equilibrium) conditions [21,22] the gravimetric information would indicate how closely the duplicate films prepared from h- and d-versions of the solvent or polymer matched each other in terms of the amounts of polymer and solvent present. In other cases, when probing the dynamics of vapour induced swelling [24], the gravimetric data could have been used to see if there was a time lag between the solvent uptake and the polymer swelling and so provide interesting information about the slow timescale polymer dynamics in thin film interfaces.

Importantly, here we have discussed the experimental precautions that need to be taken for this combination of measurements to be valid. For example, for a simple interpretation of the Love wave data it is necessary that: (i) the films must not be too thick (this thickness coincides with the upper thickness of films generally studied using NR and X-ray reflectivity); (ii) the films should have sufficiently low viscoelastic losses, and (iii) the temperature of the samples should be well controlled. If these requirements cannot be met, the technique can still be used, but the data analysis is significantly more complicated.

With these caveats in mind, the possibility of combining Love wave and reflectivity measurements will be advantageous in interfacial studies of thin films that are in *solution* as well as vapour environments. Such systems could include adsorbed lipids (where the amount of material on the surface as a result of an initial deposition or binding events could be independently assayed [25]), polymer growth [26] and chemical or electrochemical transformations that result in the adsorption, binding or influx/efflux of non-labellable species e.g. reactive motifs, ions or salt [3,6,27]. In addition, the underlying methodology of the combined NR/Love wave measurements could be expanded to be used with these and other systems when they are probed with techniques such as X-ray reflectivity and ellipsometry (where the combination with Love waves have recently been used to measure variations in the rheology of titania films during water absorption [28]).

Acknowledgements

JH acknowledges the support of the EPSRC – United Kingdom grant EP/H049479/1EPSRC. The authors thank the ILL for provision of neutron beam time and the James Watt Nanofabrication facility at Glasgow for use of equipment to make the Love wave devices.

Appendix A. Supplementary material

Supplementary data associated with this article can be found, in the online version, at http://dx.doi.org/10.1016/j.jcis.2016.10.039. Data are openly available from the University of Glasgow at http://dx.doi.org/10.5525/gla.researchdata.365.

References

[1] J. Penfold, R.K. Thomas, H.-H. Shen, Adsorption and self-assembly of biosurfactants studied by neutron reflectivity and small angle neutron scattering: glycolipids, lipopeptides and proteins, Soft Matter 8 (3) (2012) 578–591.
[2] M. Fernandez, J. Higgins, J. Penfold, Neutron reflection studies at polymer–polymer interfaces, in: Makromolekulare Chemie. Macromolecular Symposia, Wiley Online Library, 1992, pp. 103–118.
[3] A. Glidle, L. Bailey, C.S. Hadyoon, A.R. Hillman, A. Jackson, K.S. Ryder, P.M. Saville, M.J. Swann, J.R. Webster, R.W. Wilson, Temporal and spatial profiling of the modification of an electroactive polymeric interface using neutron reflectivity, Anal. Chem. 73 (22) (2001) 5596–5606.
[4] P.D. Topham, A. Glidle, D.T.W. Toolan, M.P. Weir, M. Skoda, R.D. Barker, J.R. Howse, The relationship between charge density and polyelectrolyte brush profile using simultaneous neutron reflectivity and in situ attenuated total internal reflection FTIR, Langmuir 29 (20) (2013) 6068–6076.
[5] M.P. Weir, S.Y. Heriot, S.J. Martin, A.J. Parnell, S.A. Holt, J.R. Webster, R.A. Jones, Voltage-induced swelling and deswelling of weak polybase brushes, Langmuir 27 (17) (2011) 11000–11007.
[6] A. Glidle, P.E. Pearson, E.L. Smith, J.M. Cooper, R. Cubitt, R.M. Dalgliesh, A.R. Hillman, K.S. Ryder, Determining compositional profiles within conducting polymer films following reaction with vapor phase reagents, J. Phys. Chem. B 111 (16) (2007) 4043–4053.
[7] H. Arwin, R. Jansson, Line-shape analysis of ellipsometric spectra on thin conducting polymer films, Electrochim. Acta 39 (2) (1994) 211–215.
[8] R. Cubitt, T. Saerbeck, R.A. Campbell, R. Barker, P. Gutfreund, An improved algorithm for reducing reflectometry data involving divergent beams or non-flat samples, J. Appl. Crystallogr. 48 (6) (2015).

[9] M. Strobl, R. Steitz, M. Kreuzer, M. Rose, H. Herrlich, F. Mezei, M. Grunze, R. Dahint, BioRef: a versatile time-of-flight reflectometer for soft matter applications at Helmholtz-Zentrum Berlin, Rev. Sci. Instrum. 82 (5) (2011) 055101.
[10] F.L. Dickert, P.A. Bauer, The detection of halogenated hydrocarbons via host–guest chemistry—a mass-sensitive sensor study with QMB-and SAW-devices, Adv. Mater. 3 (9) (1991) 436–438.
[11] A. Afzal, N. Iqbal, A. Mujahid, R. Schirhagl, Advanced vapor recognition materials for selective and fast responsive surface acoustic wave sensors: a review, Anal. Chim. Acta 787 (2013) 36–49.
[12] G.L. Harding, J. Du, Design and properties of quartz-based Love wave acoustic sensors incorporating silicon dioxide and PMMA guiding layers, Smart Mater. Struct. 6 (6) (1997) 716.
[13] W. Wang, S. He, Theoretical analysis on response mechanism of polymer-coated chemical sensor based Love wave in viscoelastic media, Sensors Actuat. B: Chem. 138 (2) (2009) 432–440.
[14] H. Wohltjen, A.W. Snow, W.R. Barger, D.S. Ballantine, Trace chemical vapor detection using SAW delay line oscillators, IEEE Trans. Ultrason., Ferroelect., Freq. Control 34 (2) (1987) 172–178.
[15] S. Souheib Chebil, G. Vignaud, Y. Grohens, O. Konovalov, M.K. Sanyal, T. Beuvier, A. Gibaud, In situ X-ray reflectivity study of polystyrene ultrathin films swollen in carbon dioxide, Macromolecules 45 (16) (2012) 6611–6617.
[16] T. Koga, Y.S. Seo, Y. Zhang, K. Shin, K. Kusano, K. Nishikawa, M.H. Rafailovich, J. C. Sokolov, B. Chu, D. Peiffer, R. Occhiogrosso, S.K. Satija, Density-fluctuation-induced swelling of polymer thin films in carbon dioxide, Phys. Rev. Lett. 89 (2002) 125506.
[17] H. Wohltjen, Mechanism of operation and design considerations for surface acoustic wave device vapour sensors, Sensors Actuat. 5 (4) (1984) 307–325.
[18] R. Cubitt, G. Fragneto, D17: the new reflectometer at the ILL, Appl. Phys. A 74 (1) (2002) s329–s331.
[19] D.J. Gillich, A. Kovanen, Y. Danon, Deuterated target comparison for pyroelectric crystal D-D nuclear fusion experiments, J. Nucl. Mater. 405 (2) (2010) 181–185.
[20] J.E. Mark, Physical Properties of Polymers Handbook, Springer, 1996.
[21] J. Perlich, V. Korstgens, E. Metwalli, L. Schulz, R. Georgii, P. Muller-Bushbaum, Solvent content in thin spin-coated polystyrene homopolymer films, Macromolecules 42 (2009) 337–344.
[22] X. Zhang, K.G. Yager, S. Kang, N.J. Fredin, B. Akgun, S. Satija, J.F. Douglas, A. Karim, R.L. Jones, Solvent retention in thin spin-coated polystyrene and poly (methyl methacrylate) homopolymer films studied by neutron reflectometry, Macromolecules 43 (2010) 1117–1123.
[23] P. Steward, J. Hearn, M. Wilkinson, An overview of polymer latex film formation and properties, Adv. Colloid Interface Sci. 86 (3) (2000) 195–267.
[24] P. Muller-Buschbaum, E. Bauer, E. Maurer, A. Nelson, R. Cubitt, In-situ neutron reflectometry probing competitive swelling and de-swelling of thin polystyrene films, Phys. Stat. Sol. 1 (2) (2007) R68–R70.
[25] G. Fragneto-Cusani, Neutron reflectivity at the solid/liquid interface: examples of applications in biophysics, J. Physics-Conden. Matter 13 (21) (2001) 4973–4989.
[26] M. Krishnamoorthy, S. Hakobyan, M. Ramstedt, J.E. Gautrot, Surface-initiated polymer brushes in the biomedical field: applications in membrane science, biosensing, cell culture, regenerative medicine and antibacterial coatings, Chem. Rev. 114 (21) (2014) 10976–11026.
[27] A. Glidle, J. Cooper, A.R. Hillman, L. Bailey, A. Jackson, J.R.P. Webster, Redox controlled partition and spatial distribution of solvent and salt in electroactive polyvinylferrocene films, Langmuir 19 (19) (2003) 7746–7753.
[28] L. Blanc, A. Tetelin, C. Boissière, G. Tortissier, C. Dejous, D. Rebière, Love wave characterization of the shear modulus variations of mesoporous sensitive films during vapor sorption, IEEE Sens. J. 12 (5) (2012) 1442–1449.